Relativistic effects in photoionizing a circular Rydberg state in the optical regime

Tor Kjellsson Lindblom,[1,2] Morten Førre,[3] Eva Lindroth,[4] and Sølve Selstø[1]

[1]*Faculty of Technology, Art and Design, OsloMet – Oslo Metropolitan University, NO-0130 Oslo, Norway*
[2]*PDC Center for High Performance Computing, KTH Royal Institute of Technology, SE-100 44 Stockholm, Sweden*
[3]*Department of Physics and Technology, University of Bergen, NO-5020 Bergen, Norway*
[4]*Department of Physics, Stockholm University, SE-106 91 Stockholm, Sweden*

We study the photoionization process of a hydrogen atom initially prepared in a circular Rydberg state. The atom is exposed to a two-cycle laser pulse with a central wavelength of 800 nm. Before the atom approaches saturation, at field intensities of the order of 10^{17} W/cm^2, relativistic corrections to the ionization probability are clearly seen. The ionization is predominantly driven by the radiation pressure in the propagation direction of the laser field, not by the electric field. Direct comparisons with the full numerical solution of the time-dependent Dirac equation demonstrate quantitative agreement with a semi-relativistic approximation, which is considerably easier to implement.

I. INTRODUCTION

Experiments in atomic and optical physics are about to enter an intensity regime in which the electrons involved are driven towards relativistic speeds. Thus, theoretical and computational studies must account for relativistic effects in order to be relevant. A fully relativistic description of the laser matter interaction for a fermionic system requires the solution of the time-dependent Dirac equation. In spite of the growing experimental interest, comparatively few works involving the full solution of this equation are, however, seen in the literature. This is owing to the fact that the time-dependent Dirac equation is notoriously hard to solve – for a number of reasons [1–3].

As a consequence of the complexity inherent in describing atoms exposed to strong laser fields, many studies resort to models of reduced dimensionality or approximations such as the *dipole approximation* or the *strong field approximation*. While the former approximation neglects the spatial dependence of the laser field, and, thus, also the magnetic interaction, the latter neglects the influence of the Coulomb potential during interaction with the strong laser field. Nonetheless, we have seen several notable contributions when it comes to solving the time-dependent Dirac equation numerically, see, e.g., [4–8]. And numerical solutions of the time-dependent Dirac equation in full dimensionality beyond the dipole approximation have been reported for atoms exposed to fields in the x-ray and extreme ultra violet regions, see, e.g., [3, 9, 10], and in the optical and infrared regions, see, e.g., [11–13].

Recently proposed alternative formulations of the light-matter interaction have contributed significantly in facilitating computational studies. The so-called *propagation gauge* [14–17] provides a formulation of the interaction which is numerically favourable. This is particularly so for its relativistic version as it, to a large extent, removes problems related to the inclusion of the spatial dependence of the laser field [18]; for a multipolar expansion of the light-matter interaction in the usual minimal coupling formulation, this is in fact quite involved [3]. Moreover, it has also been shown that relativistic effects induced by the external laser field may be incorporated in a non-relativistic framework by substituting the electron mass by its effective relativistic mass in the adequate manner [19]. This, in turn, allows us to study relativistic effects within a slightly modified Schrödinger equation, which requires far less effort in terms of implementation and computational power than does the Dirac equation. Previously, such semi-relativistic approaches have provided quantitative agreement with the fully relativistic calculations both in the ultra violet and x-ray regions [10, 17, 19].

Here we present results pertaining to a laser field on the border between infrared and optical wavelengths – at 800 nm. We will, by direct comparison with the numerical solution of the Dirac equation, demonstrate that quantitatively accurate results are obtained within the semi-relativistic approach also in this case.

We take our initial state to be a circular Rydberg state, i.e., a highly excited state in which both the angular and magnetic quantum numbers are maximal. In a non-relativistic context this means that $\ell = m_\ell = n - 1$. While relativistic corrections to the total hydrogen ground state photoionization probability are seen in the ultra violet region [3], such effects are harder to reveal at optical and infrared wavelengths. The reason is simply that with increasing intensity, the transition rate tends to saturate before the onset of relativistic effects in these regimes. However, for an atom initially prepared in a highly excited state, a Rydberg atom, ionization is significantly suppressed [20]. Moreover, by preparing the atom in a circular state, the initial state becomes quite stable against de-excitation as such transitions are dipole-forbidden. Thus, looking for relativistic effects in the photoionization of such a system would seem viable – also in the optical and infrared regimes.

In experiments with atoms in the gas phase, hydrogen atoms are rarely used; typically, noble gasses are preferred. Of course, atoms with several electrons are quite different from hydrogen atoms in their ground states. However, Rydberg atoms with one single excited electron can, to a large extent, be considered hydrogen-like. The excited electron effectively sees a Coulomb-like nuclear potential of one elementary charge. By introducing modified potentials or quantum defects, discrepancies from a pure Coulomb potential may be compensated for. As the wave function of a circular Rydberg state has a very small overlap with the inner region, such discrepancies are quite moderate in the first place. Thus, select-

ing a circular Rydberg state as initial state is likely to facilitate a comparison with experiment. Furthermore, the fact that circular Rydberg states may be produced experimentally, see, e.g., [21–26], also provides reason for optimism in this regard.

In the next section, we will give a brief account for the methods employed to solve the relativistic and non-relativistic equations involved. Some details regarding the actual implementation are also provided. In Sec. III we present the findings of our numerical studies, while conclusions are drawn in Sec. IV. Atomic units, "a.u.", which are defined by choosing $\hbar$, the elementary charge e, the electron mass m and $4\pi\varepsilon_0$ as the unit of their respective quantities, are used where stated explicitly.

II. THEORY AND IMPLEMENTATION

In order to identify relativistic corrections, we solve the relevant dynamical equations, i.e., the Schrödinger equation and the Dirac equation, numerically. These equations may both be expressed as

$$i\hbar \frac{\mathrm{d}}{\mathrm{d}t}\Psi = H\Psi, \tag{1}$$

where the wave function Ψ is scalar in the non-relativistic case and a four component bi-spinor in the relativistic case. Additionally, we solve a semi-relativistic version of the Schrödinger equation in which relativistic effects are accounted for by introducing a field-dressed relativistic mass [19].

All of these equations are solved within the so-called *long wavelength approximation* (LWA), which consists in first formulating the interaction in the so-called *propagation gauge*, and then disregarding the spatial dependence of the vector potential of the laser field [15, 16, 18]. In the propagation gauge, the canonical momentum corresponds to that of a free electron propagating in the combined electric and magnetic field of the laser – not just the electric field, as is the case for the usual minimal coupling formulation. For this reason, the magnetic interaction is preserved to leading order when we neglect the spatial dependence of the vector potential of the laser field in this gauge. Thus, this long wavelength approximation is far less restrictive than the much applied dipole approximation, in which the magnetic field is neglected altogether.

The LWA Hamiltonians H for which we solve Eq. (1) are

$$H_{\mathrm{NR}} = \frac{p^2}{2m} + V(r) + \frac{e}{m}\mathbf{A}\cdot\mathbf{p} + \frac{e^2 A^2}{2m^2 c}\hat{\mathbf{k}}\cdot\mathbf{p}, \tag{2a}$$

$$H_{\mathrm{SR}} = \frac{p^2}{2\mu} + V(r) + \frac{e}{\mu}\mathbf{A}\cdot\mathbf{p} + \frac{e^2 A^2}{2m\mu c}\hat{\mathbf{k}}\cdot\mathbf{p} \quad\text{and} \tag{2b}$$

$$H_{\mathrm{R}} = c\boldsymbol{\alpha}\cdot\mathbf{p} + V(r) + mc^2\beta + ce\boldsymbol{\alpha}\cdot\mathbf{A} + \frac{e^2 A^2}{2m}\hat{\mathbf{k}}\cdot\boldsymbol{\alpha}, \tag{2c}$$

for the non-relativistic case [15], the semi-relativistic case [19] and the fully relativistic case [18], respectively. Here $V(r)$ is the Coulomb potential of the nucleus, which is assumed to be of infinite mass. In the semi-relativistic

Hamiltonian of Eq. (2b) we have introduced the field-dressed mass [27, 28]

$$\mu(t) = m\left(1 + \frac{e^2}{2m^2 c^2}[A(t)]^2\right). \tag{3}$$

The semi-relativistic Hamiltonian, Eq. (2b), acts on scalar wave functions, as in the non-relativistic case, Eq. (2a). Thus, also in the semi-relativistic representation, the spin degree of freedom is neglected. For the relativistic Hamiltonian, Eq. (2c), we apply the usual representation for the α-matrices in terms of Pauli matrices,

$$\boldsymbol{\alpha} = \begin{pmatrix} 0 & \boldsymbol{\sigma} \\ \boldsymbol{\sigma} & 0 \end{pmatrix}. \tag{4}$$

The β matrix is usually represented by a block diagonal matrix with the 2×2 identity matrix I_2 in the first diagonal block and $-I_2$ in the second. However, in our implementation we have shifted the energy downwards by the rest mass energy of the electron so that it actually reads

$$\beta = \begin{pmatrix} 0 & 0 \\ 0 & -2I_2 \end{pmatrix}. \tag{5}$$

The unit vector $\hat{\mathbf{k}}$ is the propagation direction of the laser pulse. In our case, we take this direction to be along the x-axis, and the field is linearly polarized along the z-axis. The duration of the pulse corresponds to two optical cycles. Specifically, we model the laser field by

$$\mathbf{A}(t) = \frac{E_0}{\omega}\hat{\mathbf{z}}\sin^2(\omega t/4)\sin(\omega t) \tag{6}$$

for $t \in [0, 4\pi/\omega \text{ a.u.}]$; it is zero at all other times. The central angular frequency is $\omega = 0.057$ a.u., which corresponds to a wavelength of 800 nm.

It is worth emphasizing that, while we have imposed the LWA in the present work, the propagation gauge formulations do not rely on the applicability of this approximation. With a spatially dependent vector potential, the Hamiltonians of both Eq. (2a) and (2c) assume a form which differ only slightly from the LWA formulations. This form, in turn, may be obtained by imposing the gauge transformation

$$\mathbf{A} \to \mathbf{A} + \nabla\xi, \quad \varphi \to \varphi - \frac{\partial}{\partial t}\xi \quad\text{where}$$

$$\xi(\eta) = -\frac{mc^2}{2e\omega}\int_{-\infty}^{\eta}\left(\frac{eA(\eta')}{mc}\right)^2 d\eta', \tag{7}$$

$$\eta \equiv \omega t - \mathbf{k}\cdot\mathbf{r},$$

within the minimal coupling formulation, and, as such, it is mathematically equivalent to the conventional interaction form. For details on the propagation gauge formulations of the laser-matter interactions – and how they are obtained, we refer the reader to Refs. [15, 16, 18].

In arriving at the semi-relativistic interaction form, Eq. (2b), we may take the relativistic expression for the kinetic energy,

$$T = \sqrt{m^2 c^4 + p^2 c^2} - mc^2, \tag{8}$$

as our starting point. As explained in Ref. [19], if the gauge transformation (7) is now imposed, the resulting Hamiltonian reads

$$H = \mu c^2 \left(\sqrt{1 + \left(\frac{q}{\mu c} \right)^2} - 1 \right) + V(r) =$$

$$V(r) + \frac{q^2}{2\mu} - \frac{q^4}{8\mu^3 c^2} + ... \qquad (9)$$

where

$$q^2 = p^2 + 2e\mathbf{A} \cdot \mathbf{p} + \frac{e^2 A^2}{mc} \hat{\mathbf{k}} \cdot \mathbf{p} \qquad (10)$$

within the LWA. Eq. (2b) is obtained by retaining only the first two terms in Eq. (9). For total ionization probabilities in the ultra violet region, such a truncation at lowest order in $(q/\mu c)^2$ has been shown to be adequate [19], while calculations in the x-ray regime required also next order contributions in order to produce photo electron spectra in quantitative agreement with the Dirac equation [10, 17].

In all three approaches, the non-relativistic, the semi-relativistic and the fully relativistic one, Eq. (1) is solved within a spectral basis. We use the same numerical basis for the non-relativistic and the semi-relativistic approaches. The eigenstates of the unperturbed part of the Hamiltonian, H_0, are, as in previous studies [3, 18, 19], found numerically by an expansion in B-splines for the radial part and spherical harmonics for the angular part. The latter allows for an algebraic approach which enables us to significantly reduce the memory requirement for the stored information of the coupling elements by exploiting the Wigner-Eckhart theorem. In the non-relativistic case, all transition matrix blocks between symmetries with fixed angular momenta, i.e., $\ell \rightarrow \ell'$, are identical up to a scaling factor that depends on the $m_\ell \rightarrow m'_\ell$ transition. The same holds true in the relativistic case with a slight modification due to the two radial components [3, 29].

The propagation is performed using an Arnoldi propagator, i.e., a Magnus propagator approximated numerically by projection onto a Krylov subspace [30–32]. We choose the number of time-steps per optical cycle such that it requires a Krylov sub-space of maximum dimension 15 per step in the non-relativistic and semi-relativistic calculations and about 30 for the Dirac equation, which in our experience gives a robust and yet time efficient propagation. For further details, see Refs. [3, 18]. Our propagators use a hybrid parallelization strategy, in which all associated objects are distributed in nested MPI communicators. The bulk of work consists of the local matrix-vector products between distributed couplings and corresponding parts of the time dependent state vector. Due to the factorization of couplings described above, multiple matrix-vector products are now simultaneously accounted for by blocking them into matrix-matrix products. This in itself reduces the computational load significantly, and it is further boosted by using a threaded version of the Intel Math Kernel Library. For further technical details, the reader is referred to Ref. [29].

As mentioned, solving Eq. (1) with the Dirac Hamiltonian, Eq. (2c), is considerably more involved than with the Schrödinger Hamiltonian, Eq. (2a). This is not only due to the fact that the wave function has four components; another complicating factor is the stiffness induced by the mass term, i.e., the third term in Eq. (2c). For this reasons, several propagation schemes are subjected to the requirement that the numerical time-step must be even lower than the inverse of the mass energy splitting, $\Delta t < 1/(2mc^2)$. This severe restriction may, however, be evaded by applying a propagator of Magnus form [31].

When it comes to implementing calculations involving the semi-relativistic formulation, Eq. (2b), the complexity is more or less the same as in the non-relativistic case. The two last interaction terms in Eq. (2b) differ only from those of Eq. (2a) in the time-dependent prefactors. The coupling originating from the field-induced relativistic modification of the kinetic energy is conveniently calculated in our spectral basis as

$$\frac{p^2}{2m} \left(\frac{m}{\mu(t)} - 1 \right) = \left(\frac{m}{\mu(t)} - 1 \right) (H_0 - V(r)), \qquad (11)$$

where the time-independent part

$$H_0 = \frac{p^2}{2m} + V(r) \qquad (12)$$

is diagonal in our basis, and the coupling elements of the isotropic Coulomb potential $V(r)$ are rather easily obtained.

For both the non-relativistic and semi-relativistic calculations we achieved converged results within a numerical domain extending up to a distance of $r_{\max} = 1600$ a.u. from the nucleus. Such a large domain is necessary not only in order to contain the wave function, which has a rather large excursion amplitude, but also in order to obtain a sufficiently precise distinction between Rydberg states and (pseudo) continuum states in the spectral basis. Within this radial domain, B-splines of order seven with a uniformly distributed knot sequence with a spacing of 1 a.u. for each knot was used. In order to avoid artificial reflections of high-energy components, a complex absorbing potential was imposed close to the numerical boundary. For the angular part, we used partial waves with maximum angular quantum number $\ell_{\max} = 200$ and included all magnetic quantum numbers, giving 40401 angular symmetries for the Schrödinger equation and twice as much for the Dirac equation. States with eigenenergies beyond 50 a.u. where removed from the spectral basis.

For the numerical solution of the Dirac equation, we used the same numerical parameters as for the Schrödinger equations – with certain adjustments. In solving the time-independent Dirac equation, i.e., obtaining the eigenstates of Eq. (2c) with $A = 0$, we expanded the radial part of the lower spinor in B-splines of order eight – as opposed to seven in the case of the upper spinor. This was done in order to avoid contamination of the spectrum by so-called spurious states [33]. As the Dirac Hamiltonian, contrary to the Schrödinger Hamiltonian, is unbounded from below, we imposed energy truncation in both ends of the spectrum; in addition to removing pseudo continuum states beyond 50 a.u., we also removed states of energy below $-2mc^2 - 50$ a.u. It is worth emphasizing that, in spite of the large energy separation, a full trunca-

tion of the negative energy continuum is not admissible, see, e.g., Refs. [1, 2].

The computational load is quite severe. The number of basis functions is roughly $6.4 \cdot 10^7$ and $2.6 \cdot 10^8$ for the non-relativistic and relativistic cases, respectively. The aforementioned factorization of angular couplings reduces the stored coupling information from 4.8 TB to 8 GB in the non-relativistic case and from 76.8 TB to 128 GB in the relativistic case. The largest simulations were carried out on the supercomputer Fram in Tromsø, Norway, employing 2208 cpu-cores for about a week. In terms of the total number of required operations, the semi-relativistic propagator is roughly 30 times lighter than the fully relativistic propagator signifying the benefit of being able to use the former version.

Finally, it should be noted that the angular quantum numbers ℓ and m_ℓ are not actually good quantum numbers for the unperturbed Dirac Hamiltonian. However, for a state with total angular quantum numbers j and m_j both equal to $\ell+1/2$, the upper, large component of the solution of the time-independent Dirac equation does have well defined ℓ and m_ℓ values; when solving the time-dependent Dirac equation, we take our initial state to be such a state. Specifically, when resolving the dynamics, i.e., solving Eq. (1) with the Hamiltonians of Eqs. (2), our initial Rydberg state has principal quantum number $n = 11$. Our circular state has angular quantum numbers $\ell = m_\ell = 10$ in the non-relativistic and semi-relativistic cases and $j = m_j = 21/2$ ($\kappa = -11$) in the fully relativistic case.

III. RESULTS AND DISCUSSION

Figure 1 shows the ionization probability as a function of the maximum intensity of the laser pulse. Only two data points originates from the solution of the Dirac equation. The reason for this is the high demand on computational resources, as discussed above. In our calculations, the highest peak electric field strength is $E_0 = 3$ a.u., which corresponds to about $3.2 \cdot 10^{17}$ W/cm^2 in intensity. According to a classical estimate of the maximum quiver velocity of a free electron, $v_{\mathrm{quiv}} = eE_0/m\omega$, this corresponds to about 38 % of the speed of light. At peak intensity, the field dressed mass μ, cf. Eq. (3), exceeds the rest mass by 7 %. Thus, it should come as no surprise that we do see relativistic corrections at this intensity.

Another interesting observation is that the ionization probability as predicted by the semi-relativistic approach with the Hamiltonian of Eq. (2b) agrees very well with the fully relativistic calculations; this is particularly evident from the lower panel of Fig. 1, which depicts the difference between the relativistic and non-relativistic ionization yields. For $E_0 = 3$ a.u., the correction predicted by the semi-relativistic approach differs by less than one percent from the fully relativistic correction. By including the next to leading order in Eq. (9), this relative error is reduced to 0.2 %.

It is thus clear that the semi-relativistic approach is indeed able to provide the correct relativistic ionization probability. This, in turn, implies that neither spin-effects nor relativistic corrections to the spectrum of the atom affect the total yield
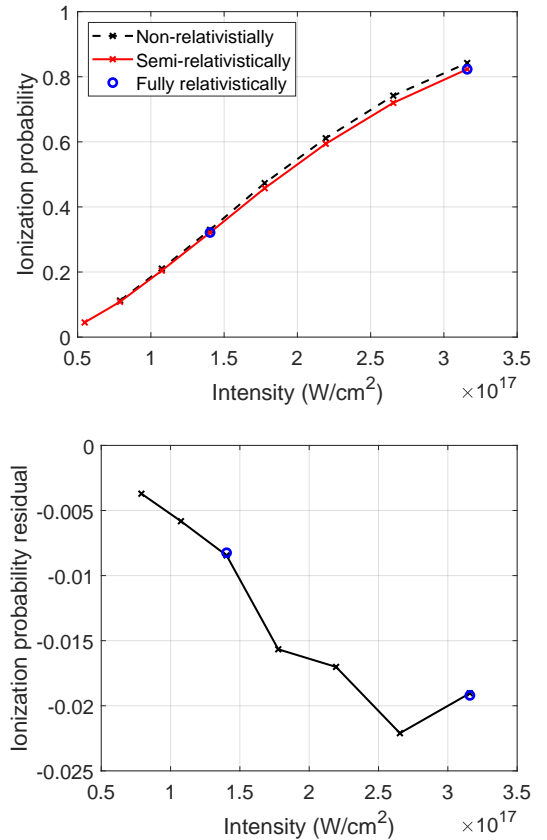

FIG. 1: The upper panel shows the ionization probability for a hydrogen atom initially prepared in the circular Rydberg state with $n = 11$ exposed to a two-cycle laser pulse as a function of the peak intensity of the laser. The central wavelength of the laser is 800 nm. The dashed curve is obtained with the Schrödinger equation, i.e., with the Hamiltonian of Eq. (2a), while the full curve is calculated with the semi-relativistic version, Eq. (2b). The circular data points are obtained from full solutions of the Dirac equation, i.e., with the Hamiltonain of Eq. (2c). In all cases, the so-called *long wavelength approximation* is applied. In the lower panel, the difference between the non-relativistic and the relativistic results are plotted.

significantly for this setup. Since the semi-relativistic description, Eq. (2b), effectively amounts to a dynamic increase in the inertia of the electron, this is indeed the most important relativistic correction. It is seen in Fig. 1 that the increased inertia consistently leads to an ionization probability which is lower than the non-relativistic one; as in Refs. [3, 19] we find that relativistic effects tend to somewhat stabilize the atom against ionization. This has also been seen in a one-dimensional model of photoionization from the ground state [34]. The lower panel of Fig. (1) shows that the effect is not entirely monotonic; initially, the correction increases with increasing intensity as relativistic effects start to become significant. As the system at higher intensities approaches saturation, both according to relativistic and non-relativistic calculations, the difference in ionization probability is seen to decrease again.

It is worth noting that the much applied dipole approximation fails completely in predicting these ionization yields.
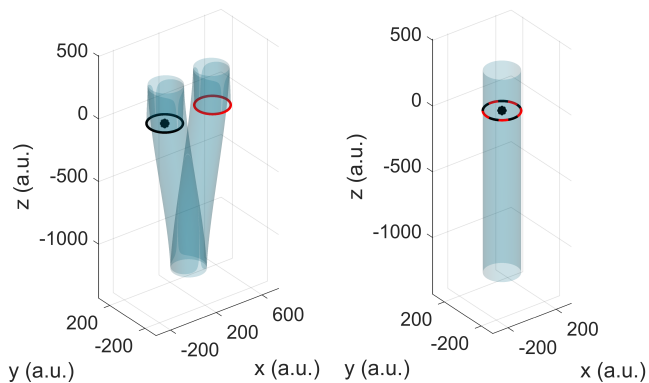
FIG. 2: Left panel: The classical translation of an initial circular Rydberg "state", illustrated by a black ring, imposed by a two-cycle laser field of maximum electric field strength $E_0 = 3$ a.u. The black dot illustrates the position of the nucleus, whose influence is disregarded in this illustration. The red circle marks the resulting position. While the electric component imposes a strong excursion during interaction with the pulse, there is no net translation in the polarization direction (z-axis) after the interaction. The radiation pressure, on the other hand, pushes the electron far into the propagation direction (x-axis). Within the dipole approximation, there is no such push, and the initial and final positions coincide (right panel).

Calculations we have performed within the dipole approximation turn out to underestimate the ionization probability by orders of magnitude for these intensities. Since the dipole approximation disregards magnetic interactions altogether, its inapplicability should come as no surprise. It is well known that the magnetic interaction contributes significantly to the dynamics of atoms in strong fields in the optical and infrared regions – both from theoretical considerations [27, 35–38], other numerical studies [11, 20] and from experiment [13, 39–43]. However, since electric interactions tend to dominate magnetic interactions, it may be surprising to see the dipole approximation fail this miserably. For instance, if we assume that the electron's momentum is about 0.1 a.u. in both the polarization and the propagation direction, the dipole interaction term $e/m\, A(t) p_z$ amounts to an energy of 5.26 a.u. at peak intensity, while the radiation pressure term $e^2/(2m^2c)\,[A(t)]^2 p_x$ would contribute about 1.01 a.u., i.e., the former exceeds latter by about a factor 5. When the last term still provides the dominant ionization mechanism, this is related to the fact that the dipole part of the interaction corresponds to a zero-displacement pulse; although subjected to a strong driving, a free, classical electron would experience no net displacement in the polarization direction after being exposed to the electric field provided by the vector potential in Eq. (6) [44]. The combined action of the electric and the magnetic fields, however, provides a radiation pressure which is non-oscillatory; for each half-cycle it pushes the electron in the positive propagation direction [45]. This effect is precisely what the last term of each of the Hamiltonians in Eqs. (2) account for. Our numerical results suggest that this displacement effect is the dominant ionization mechanism. For illustration, we show the dynamical displacement imposed by the pulse on a classical, free electron in Fig. 2.
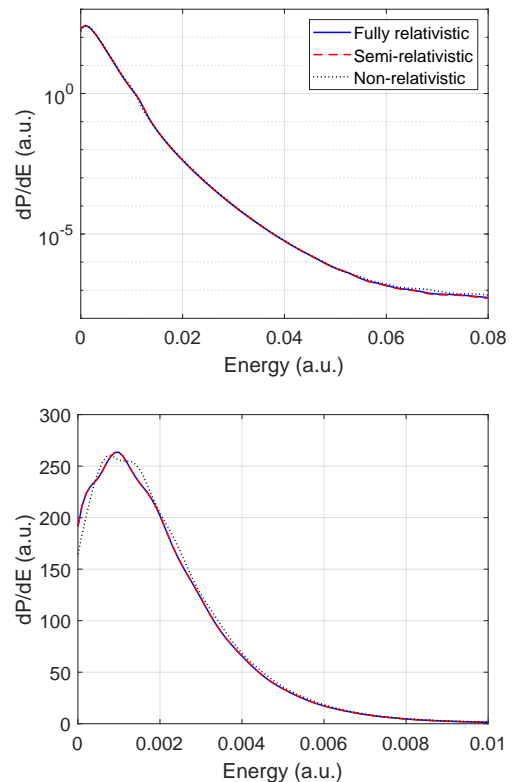

FIG. 3: The photo electron spectrum obtained from relativistic (blue full curve), semi-relativistic (red dashed) and non-relativistic (black dotted) calculations. The peak electric field strength corresponds to an intensity of $3.2 \cdot 10^{17}$ W/cm^2. In the upper panel, the spectrum is shown using a logarithmic y-axis, while the lower panel shows a close-up at the peak just above threshold using a linear y-axis.

Figure 3 shows the ionization probability differential in energy obtained with the three Hamiltonians of Eqs. (2). Again, the peak electric field strength is $E_0 = 3$ a.u. With our wave function expressed in a spectral basis, the spectra are readily obtained by interpolating the final population of each pseudo continuum state within each angular symmetry. In the upper panel we see that virtually all probability is concentrated just above threshold. The spectrum is seen to be rather monotonic; no structure corresponding to multi-photon ionization is seen. This is not only due to the comparatively short time-duration of the pulse. With an effective ionization potential of $-1/(2n^2) = 0.0041$ a.u. for $n = 11$ the Keldysh parameter $\gamma = 0.0019$ indicates that the multi-photon ionization mechanism is entirely suppressed [46]. On the other hand, the laser field is so strong that the modified Coulomb potential does not feature any barrier against ionization at all. Thus, tunneling theories such as the relativistic PPT theory, see, e.g., [47–50], are not applicable here. Rather, according to the above discussion, ionization predominantly comes about by the radiation pressure, which displaces the electron in the propagation direction of the laser pulse. In this simple picture, the laser pulse does not impose any net acceleration onto the liberated electron.

The spectra seen in the upper panel of Fig. 3 are virtually indistinguishable. A close up on the peak near threshold, however, reveals small differences between the non-relativistic calculation and the other ones. This is depicted in the lower panel of Eq. (3), where we, contrary to the upper panel, have used a linear y-axis. We do not see any difference between the relativistic and the semi-relativistic predictions. In other words, also when it comes to the photo-electron spectrum, the semi-relativistic approach provides quantitative agreement with the solution of the Dirac equation.

The spectrum is peaked at an energy of about 10^{-3} a.u. Also this can be understood from the simple semi-classical picture illustrated in Fig. 2. If the wave packet is simply displaced by the laser field, unaffected by both dispersion and diffraction, the kinetic energy of the particle is also unaffected. However, as the particle is still subject to the Coulomb potential, the total energy depends on the position. If we, as an estimate, assume that the kinetic energy of the displaced particle coincides with the mean value of the initial wave packet and average the total energy over the positions indicated by red ring depicted in the left panel of Fig. 2, we arrive at an estimated mean energy of 0.0017 a.u. The actual mean value according to the distributions depicted in Fig. 3 is 0.0021 a.u. (for both the non-relativistic and the relativistic distributions).

If we, within the same picture, also take into account that the wave packet, to a certain extent, is subject to diffraction induced by the Coulomb potential as it is driven by the laser field, we may also understand the small differences seen between the non-relativistic and the relativistic spectra in the lower panel Fig. 3. A relativistic calculation of the path followed by a classical particle would differ slightly from a non-relativistic one. Correspondingly, the wave packet experiences Coulomb-diffraction which differs slightly in the non-relativistic and relativistic calculations. This, in turn, may explain the small but distinguishable fluctuations in the respective energy distributions.

IV. CONCLUSIONS

We investigated the ionization dynamics of a hydrogen atom initially prepared in a circular Rydberg state exposed to a short laser pulse with a wavelength of 800 nm. It was seen that the dominant ionization mechanism relied on the magnetic interaction, thus rendering the dipole approximation inadequate. The laser pulse was strong enough to accelerate the electron towards a large fraction of the speed of light, and relativistic corrections to the ionization probability were found to be significant. It was also found that these relativistic corrections tend to shift the total ionization probability downwards, indicating that the increased inertia of the relativistic electron to some extent stabilizes the atom against ionization.

This explanation in terms of increased inertia is supported by quantitative agreement between fully relativistic calculations and a semi-relativistic approach in which the electron's mass is replaced by an efficient field-dressed mass. The demonstrated adequacy of this semi-relativistic approach is a very useful result indeed as it facilitates relativistic calculations considerably. It is by no means restricted to the particular laser pulse or the initial state used here, it applies to several systems in which the external field, not the internal Coulomb field, accelerates the electrons towards relativistic speeds.

[1] S. Selstø, E. Lindroth, and J. Bengtsson, Phys. Rev. A **79**, 043418 (2009).

[2] Y. V. Vanne and A. Saenz, Phys. Rev. A **85**, 033411 (2012).

[3] T. Kjellsson, S. Selstø, and E. Lindroth, Phys. Rev. A **95**, 043403 (2017).

[4] J. W. Braun, Q. Su, and R. Grobe, Phys. Rev. A **59**, 604 (1999).

[5] G. R. Mocken and C. H. Keitel, Computer Physics Communications **178**, 868 (2008).

[6] H. Bauke and C. H. Keitel, Computer Physics Communications **182**, 2454 (2011).

[7] Q. Lv, D. Jennings, J. Betke, Q. Su, and R. Grobe, Comput. Phys. Comm. **198**, 31 (2016).

[8] F. Fillion-Gourdeau, E. Lorin, and A. Bandrauk, Journal of Computational Physics **307**, 122 (2016).

[9] I. A. Ivanov, Phys. Rev. A **96**, 013419 (2017).

[10] M. Førre, Phys. Rev. A **99**, 053410 (2019).

[11] I. A. Ivanov, Phys. Rev. A **91**, 043410 (2015).

[12] I. A. Ivanov and K. T. Kim, Phys. Rev. A **92**, 053418 (2015).

[13] N. Haram, I. Ivanov, H. Xu, K. T. Kim, A. Atia-tul Noor, U. S. Sainadh, R. D. Glover, D. Chetty, I. V. Litvinyuk, and R. T. Sang, Phys. Rev. Lett. **123**, 093201 (2019).

[14] J. R. Vázquez de Aldana, N. J. Kylstra, L. Roso, P. L. Knight, A. Patel, and R. A. Worthington, Phys. Rev. A **64**, 013411 (2001).

[15] M. Førre and A. S. Simonsen, Phys. Rev. A **93**, 013423 (2016).

[16] A. S. Simonsen and M. Førre, Phys. Rev. A **93**, 063425 (2016).

[17] M. Førre and S. Selstø, Phys. Rev. A **101**, 063416 (2020).

[18] T. Kjellsson, M. Førre, A. S. Simonsen, S. Selstø, and E. Lindroth, Phys. Rev. A **96**, 023426 (2017).

[19] T. Kjellsson Lindblom, M. Førre, E. Lindroth, and S. Selstø, Phys. Rev. Lett. **121**, 253202 (2018).

[20] M. Førre, Phys. Rev. A **74**, 065401 (2006).

[21] R. G. Hulet and D. Kleppner, Phys. Rev. Lett. **51**, 1430 (1983).

[22] J. Hare, M. Gross, and P. Goy, Phys. Rev. Lett. **61**, 1938 (1988).

[23] D. Delande and J. C. Gay, Europhys. Lett. **5**, 303 (1988).

[24] S. B. Hansen, T. Ehrenreich, E. Horsdal-Pedersen, K. B. MacAdam, and L. J. Dubé, Phys. Rev. Lett. **71**, 1522 (1993).

[25] J. C. Day, T. Ehrenreich, S. B. Hansen, E. Horsdal-Pedersen, K. S. Mogensen, and K. Taulbjerg, Phys. Rev. Lett. **72**, 1612 (1994).

[26] A. A. Morgan, V. Zhelyazkova, and S. D. Hogan, Phys. Rev. A **98**, 043416 (2018).

[27] H. R. Reiss, Phys. Rev. A **19**, 1140 (1979).

[28] E. S. Sarachik and G. T. Schappert, Phys. Rev. D **1**, 2738 (1970).

[29] T. Kjellsson Lindblom, Ph.D. thesis, Stockholm University, Dept. of Physics (2017).

[30] S. Blanes, F. Casas, J. Oteo, and J. Ros, Physics Reports **470**, 151 (2009).

[31] M. Hochbruck and C. Lubich, SIAM J. Numer. Anal. **41**, 945 (2003).

[32] R. Beerwerth and H. Bauke, Comput. Phys. Comm. **188**, 189 (2015).

[33] C. F. Fischer and O. Zatsarinny, Comput. Phys. Comm. **180**, 879 (2009).

[34] N. J. Kylstra, A. M. Ermolaev, and C. J. Joachain, J. Phys. B **30**, L449 (1997).

[35] M. Klaiber, E. Yakaboylu, H. Bauke, K. Z. Hatsagortsyan, and C. H. Keitel, Phys. Rev. Lett. **110**, 153004 (2013).

[36] P.-L. He, D. Lao, and F. He, Phys. Rev. Lett. **118**, 163203 (2017).

[37] J. c. v. Daněk, K. Z. Hatsagortsyan, and C. H. Keitel, Phys. Rev. A **97**, 063409 (2018).

[38] H. Ni, S. Brennecke, X. Gao, P.-L. He, S. Donsa, I. Březinová, F. He, J. Wu, M. Lein, X.-M. Tong, et al., Phys. Rev. Lett. **125**, 073202 (2020).

[39] C. T. L. Smeenk, L. Arissian, B. Zhou, A. Mysyrowicz, D. M. Villeneuve, A. Staudte, and P. B. Corkum, Phys. Rev. Lett. **106**, 193002 (2011).

[40] A. Ludwig, J. Maurer, B. W. Mayer, C. R. Phillips, L. Gallmann, and U. Keller, Phys. Rev. Lett. **113**, 243001 (2014).

[41] J. Maurer, B. Willenberg, J. Daněk, B. W. Mayer, C. R. Phillips, L. Gallmann, M. Klaiber, K. Z. Hatsagortsyan, C. H. Keitel, and U. Keller, Phys. Rev. A **97**, 013404 (2018).

[42] A. Hartung, S. Eckart, S. Brennecke, J. Rist, D. Trabert, K. Fehre, M. Richter, H. Sann, S. Zeller, K. Henrichs, et al., Nature Physics **15**, 1222 (2019).

[43] B. Willenberg, J. Maurer, B. W. Mayer, and U. Keller, Nature Comm. **10**, 5548 (2019).

[44] I. A. Ivanov, A. S. Kheifets, K. Bartschat, J. Emmons, S. M. Buczek, E. V. Gryzlova, and A. N. Grum-Grzhimailo, Phys. Rev. A **90**, 043401 (2014).

[45] D. Dimitrovski, M. Førre, and L. B. Madsen, Phys. Rev. A **80**, 053412 (2009).

[46] L. V. Keldysh, Sov. Phys. JETP **20**, 1307 (1965).

[47] V. D. Mur, B. M. Karnakov, and V. S. Popov, JETP **87**, 433 (1998).

[48] N. Milosevic, V. P. Krainov, and T. Brabec, Journal of Physics B: Atomic, Molecular and Optical Physics **35**, 3515 (2002).

[49] N. Milosevic, V. P. Krainov, and T. Brabec, Phys. Rev. Lett. **89**, 193001 (2002).

[50] V. S. Popov, B. M. Karnakov, and V. D. Mur, JETP Lett. **79**, 262 (2004).